inorganics

MDPI

Article

Different Patterns of Pd-Promoted C-H Bond Activation in (*Z*)-4-Hetarylidene-5(4*H*)-oxazolones and Consequences in Photophysical Properties

Miguel Martínez, David Dalmau, Olga Crespo, Pilar García-Orduña, Fernando Lahoz, Antonio Martín and Esteban P. Urriolabeitia *

Instituto de Síntesis Química y Catálisis Homogénea, CSIC-Universidad de Zaragoza, 50009 Zaragoza, Spain; 780460@unizar.es (M.M.); ddalmau@unizar.es (D.D.); ocrespo@unizar.es (O.C.); mpgaror@unizar.es (P.G.-O.); lahoz@unizar.es (F.L.); tello@unizar.es (A.M.)

* Correspondence: esteban.u.a@csic.es or esteban@unizar.es

Abstract: This work aims to amplify the fluorescence of (*Z*)-4-hetarylidene-5(4*H*)-oxazolones **1** by suppression of the hula-twist non-radiative deactivation pathway by CˆN-orthopalladation of the 4-hetarylidene ring. Different (*Z*)-4-hetarylidene-2-phenyl-5(4*H*)-oxazolones, **1a**–**1c**, prepared by the Erlenmeyer–Plöchl method, have been studied. The orthopalladation of (*Z*)-2-phenyl-4-(5-thiazolylmethylene)-5(4*H*)-oxazolone (**1a**) takes place by C-H bond activation of the H4 of the heterocycle and CˆN-chelation, giving the dinuclear trifluoroacetate derivative **2a**. By further metathesis of bridging ligands in **2a**, complexes containing the orthometalated oxazolone and a variety of ligands **3a**–**5a,** were prepared. The study of the photophysical properties of **1a**–**5a** shows that the bonding of the Pd metal to the 4-hetaryliden-5(4*H*)-oxazolone does not promote, in these cases, an increase in fluorescence. Interestingly, the orthopalladation of (*Z*)-2-phenyl-4-(4-thiazolylmethylene)-5(4*H*)-oxazolone (**1b**) gives orthopalladated **2b**, where the incorporation of the Pd to the oxazolone takes place by C-H bond activation of the ortho-H2 of the 2-phenyl group, ring opening of the oxazolone heterocycle and simultaneous N,N-bonding of the N atoms of the thiazole ring and the generated benzamide fragment. This NˆNˆC-tridentate dianionic bonding mode is obtained for the first time in oxazolones. Despite a similar lock of the hula-twist deactivation, **2b** does not show fluorescence.

Keywords: oxazolones; fluorescence; heterocycles; C-H bond activation; palladium

Citation: Martínez, M.; Dalmau, D.; Crespo, O.; García-Orduña, P.; Lahoz, F.; Martín, A.; Urriolabeitia, E.P. Different Patterns of Pd-Promoted C-H Bond Activation in (*Z*)-4-Hetarylidene-5(4*H*)-oxazolones and Consequences in Photophysical Properties. *Inorganics* **2024**, *12*, 271. https://doi.org/10.3390/inorganics12100271

Academic Editor: Binbin Chen

Received: 17 September 2024
Revised: 15 October 2024
Accepted: 17 October 2024
Published: 18 October 2024

1. Introduction

The synthesis of compounds with photophysical properties of interest, such as fluorescence or phosphorescence, is a well-established area of research. However, in recent years, it has been experiencing growing development due to its multiple applications. The most impactful and well-known application is their use as screens in optical devices, followed by their employment as biological markers or probes for disease detection through the visualization of the vital activity of cells and organisms [1–7].

There are various criteria to consider when designing the synthesis of a molecule with potential luminescent properties. In this regard, nature provides us with models to follow, as many natural compounds exhibit luminescent properties. A notable example is the GFP (Green Fluorescent Protein) and its derivatives. GFP has come to be commonly known as the microscope of the 21st century, due to its ease of visualizing cellular internal functioning when irradiated with UV light, which causes the emission of an intense green light. The utility of GFP and its derivatives was so significant that, in 2008, the Nobel Prize in Chemistry was awarded to Professors Shimomura, Chalfie, and Tsien [8–10].

However, the true reason for the photophysical activity of GFP is the protein's chromophore, a small molecule whose backbone contains the (*Z*)-4-arylidene-5(4*H*)-imidazolone

unit (Figure 1a), confined in the internal part of the protein in a very rigid structural environment. These GFP chromophores are formed by the internal modification of some amino acid residues. These modifications are catalyzed by the fluorescent protein itself and do not require external enzymatic activity. Recently, it has been demonstrated that GFP exhibits a wide spectral variety due to the presence of different chromophore structures [11–14].

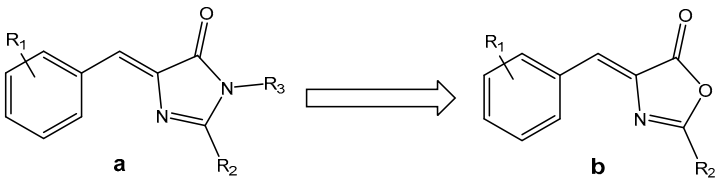

Figure 1. Structure of: (**a**) 4-aryliden-5(4*H*)-imidazolone; (**b**) 4-aryliden-5(4*H*)-oxazolone.

The 4-arylidene-5(4*H*)-oxazolone compounds, shown in Figure 1b, are structural analogs of the 4-arylidene-5(4*H*)-imidazolones and can be considered their synthetic precursors, as the imidazolones can be easily obtained from the oxazolones. Both types of compounds, oxazolones and imidazolones, are very versatile precursors in the synthesis of α-amino acids and, as expected, they also exhibit interesting photophysical properties [15]. However, it is important to note that the existence of photophysical properties of interest in the chromophores of the GFP protein is a direct consequence of the rigid environment they have inside the protein. In the absence of this rigidity, for example, in a solution outside of the protein, the luminescence disappears due to alternative relaxation processes through non-radiative pathways, known as "hula-twist" (Figure 2a) [16–21].

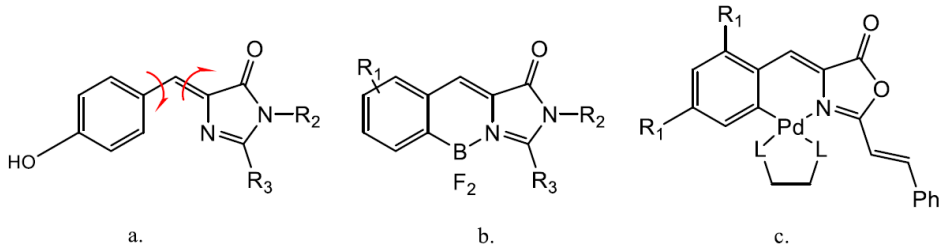

Figure 2. (**a**) "Hula-twist" relaxation (Imidazolone); (**b**) Chromophore with conformational blocking through the introduction of the BF_2 fragment (Imidazolone); (**c**) Chromophore with conformational blocking through PdL_2 (Oxazolone).

If these structures exhibit high fluorescence in a very rigid and complex environment, such as that of the protein, it is important to prevent the loss of fluorescence in non-rigid environments. Several solutions have been proposed to prevent the loss of fluorescence through non-radiative pathways, all centered on imidazolones. The most interesting of these solutions is the conformational blocking of the arylidene fragment of the heterocycle by anchoring the ortho carbon atom and the nitrogen of the heterocycle through coordination to the same molecular fragment [22,23]. The insertion of BF_2, as shown in Figure 2b, has provided spectacular results in increasing fluorescence, as it decreases the degrees of freedom and increases conformational restriction, thus minimizing the effects of non-radiative losses through hula-twist [22,23].

Subsequently, it has been shown that it is also possible to achieve this objective using palladium as an anchor, both in oxazolones and imidazolones, as shown in Figure 2c [15,24–26]. The incorporation of Pd into the oxazolone and imidazolone skeletons occurs easily through C-H bond activation. The square-planar environment of palladium additionally requires the presence of auxiliary ligands, whose steric and electronic properties also influence fluorescence. Using this type of strategy with Pd organometallics, fluorescence amplifications of up to two orders of magnitude have been obtained in certain cases when transitioning from the free ligand to the complex, with quantum yields of up to 28% [25]. All the photophysical

results discussed so far have been carried out on orthopalladated oxazolones containing a substituted 4-arylidene group. However, no study has been conducted on oxazolones that contain heterocycles in that position, that is, 4-hetarylidene groups as represented in Figure 3 (X, Y, Z in Figure 3 can be S, O, NH, CH, etc.). In particular, heterocycles such as thiazole or imidazole could be of special interest due to their well-known intrinsic luminescent properties.

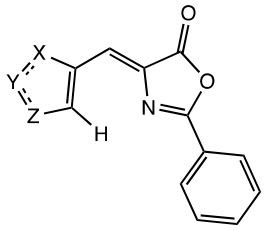

Figure 3. General structure of (*Z*)-4-hetaryliden-5(4*H*)-oxazolones (X, Y, and Z can be O, NH, or S).

Given the critical role of the arylidene fragment in the photophysical properties of oxazolones, this work addresses the synthesis and characterization of (*Z*)-4-hetarylidene-2-phenyl-5(4*H*)-oxazolones, the study of their reactivity towards Pd(II), and especially the measurement of the photophysical properties of both the free ligands and the complexes, aiming to determine if fluorescence amplification occurs after incorporating Pd into the oxazolone skeleton. It is particularly noteworthy that the study of the reactivity of particular (*Z*)-4-hetarylidene-2-phenyl-5(4*H*)-oxazolones has led to the characterization of a new type of C-H bond activation in these substrates.

2. Results and Discussion

2.1. Synthesis and Characterization of Oxazolones from Heterocycles

The oxazolones **1a**–**1c**, shown in Figure 4, were prepared from the corresponding aldehydes following the Erlenmeyer–Plöchl method described in the literature [27–33]. In the case of oxazolone **1c,** additional N-acetylation of the NH bond of the imidazole ring has been observed due to its reaction with the acetic anhydride used as reaction solvent. The presence of this acetyl group should not limit further reactivity with palladium and confers additional stability to this ring. All oxazolones **1** were obtained as yellow solids stable to air and moisture, with yields ranging from 39% to 97%. They have been selected aiming to cover various structural situations, such as N,S-heterocycles versus N,N-heterocycles and within N,S-heterocycles; we change the reactive position to observe the influence of the substitution position on the ring.

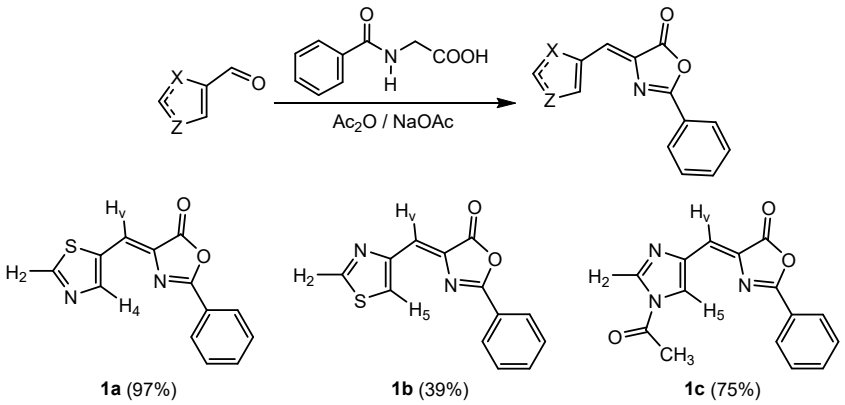

Figure 4. General synthesis of oxazolones and examples **1a**–**1c** employed in this work (yields in parentheses).

The characterization of **1a**–**1c** has been carried out by HRMS and NMR methods (see Materials and Methods section and Supplementary Materials). The HRMS spectra in all cases show the presence of a peak with the isotopic distribution corresponding to the molecular ion $[M]^+$, which has captured Na^+ $[M + Na]^+$ or K^+ $[M + K]^+$ cations. These results confirm the stoichiometries shown in Figure 4. The ^1H and ^{13}C NMR spectra of **1a**–**1c** show characteristic signals that suggest the structures of the oxazolones depicted in Figure 4. The ^1H-NMR spectrum of **1a** shows two doublets of doublets at 9.05 and 8.32 ppm, assigned to the hydrogens of the 5-thiazole heterocycle, H2 and H4, respectively. Meanwhile, the H2 and H5 protons of the 4-thiazolyl group in **1b** appear as two doublets at 8.88 and 8.80 ppm, and those corresponding to the imidazole group in **1c** appear at 8.54 ppm (H2) and 8.21 ppm (H5). The ^1H-NMR spectrum of **1c** also shows the presence of a singlet at 2.70 ppm, integrating for 3H. This singlet correlates in the ^1H-^{13}C HMBC with a carbonyl group at 165.88 ppm and with a methyl group at 22.70 ppm in the ^1H-^{13}C HSQC. These findings confirm the presence of the acetyl group –C(O)Me in the molecule. Signals due to H belonging to the Ph group and the vinyl proton appear as expected. Similarly, the $^{13}C\{^1H\}$ NMR spectrum of **1a** shows peaks at 159.62, 149.26, and 132.28 ppm, which are characteristic of the C2, C4, and C5 carbons, respectively, of the 5-substituted thiazole ring. The formation of the oxazolone heterocycle is inferred from the observation of signals at 165.82 ppm, assigned to the C=O group, 163.47 ppm (C=N group), and a third at 133.22 ppm due to the quaternary carbon of the arylidene group. The signal corresponding to the vinylic carbon is located at 120.97 ppm. This analysis is similarly applicable to **1b** and **1c**.

The determination of the molecular structure of oxazolone **1c** by X-ray diffraction, depicted in Figure 5, provides additional structural information. Crystals of compound **1c** were obtained by slow diffusion of *n*-pentane into a solution of the crude compound in CH_2Cl_2 at −18 °C over the course of one week. The Supplementary Materials includes the main crystallographic data related to data collection, and the process of solving and refining **1c**.

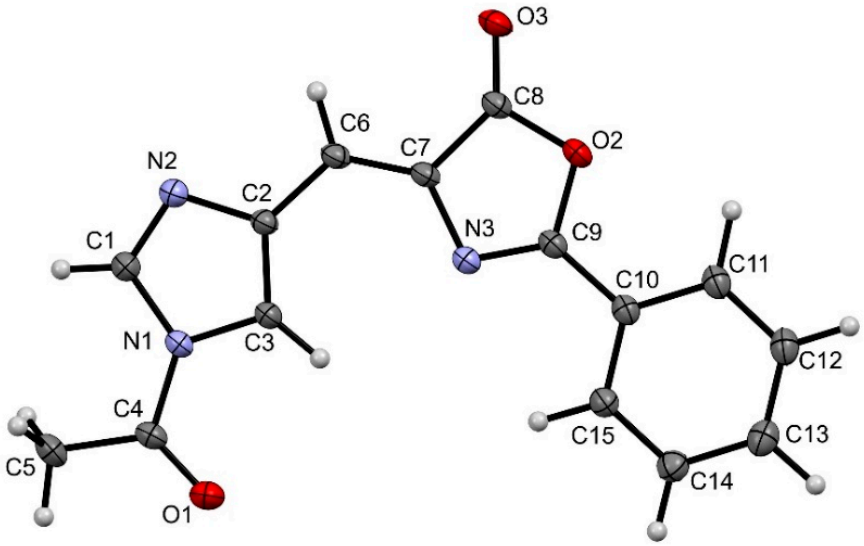

Figure 5. Molecular structure of oxazolone **1c**. Thermal ellipsoids are drawn at 50% probability level.

The structure clearly shows the formation of the 5(4*H*)-oxazolone ring, substituted at position 2 by a phenyl group and at position 4 by an *N*-acetyl-imidazolidene group, which in turn confirms the substitution of the NH proton of the imidazole group by an acetyl group, as the NMR spectra suggested. The configuration of the C=C double bond is (*Z*), as is typical in oxazolones [34,35]. A comparison of bond lengths and angles of this oxazolone with values found for other unsaturated oxazolones reported in the literature shows that

the presence of the heterocycle on the exocyclic vinylic carbon does not cause deviations in the oxazolone ring [36].

*2.2. C-H Bond Activation Reactions: Synthesis and Characterization of the Orthometalated Dinuclear Pd Complex with Trifluoroacetate Bridges (**2a**) and the Tridentate Complex (**2b**)*

Once the oxazolones were characterized, their reactivity with $Pd(OAc)_2$ was tested with the aim of incorporating Pd into the molecular skeleton of the oxazolone and restricting possible fluorescence deactivation pathways. The incorporation of Pd into the oxazolone skeleton **1a** is achieved by orthometalation through a C-H activation process, described in the literature [24–26,36–39], which generates the dinuclear complex with trifluoroacetate bridges **2a** (55% yield) shown in Scheme 1.

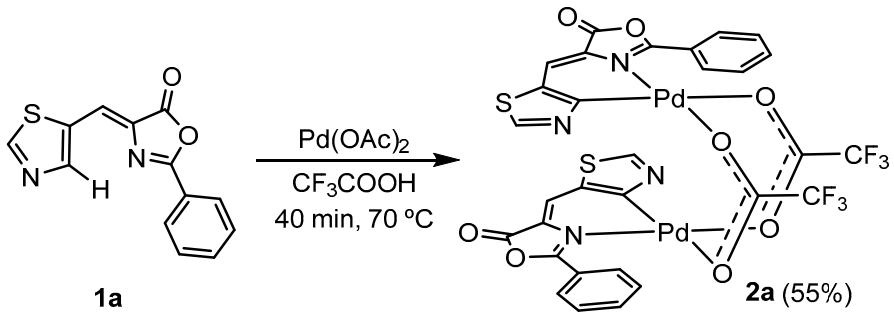

Scheme 1. Synthesis of dinuclear orthopalladated complex **2a** through CH bond activation.

Heating the mixture of **1a** and $Pd(OAc)_2$ in trifluoroacetic acid at 70 °C causes the initial suspension to change color to a more intense brown. After 40 min heating, the addition of water to the cool suspension causes more solid to precipitate. This solid is filtered and washed with water to remove the excess of acid. This solid contains complex **2a** contaminated with black Pd^0. Therefore, it is then recrystallized by adding CH_2Cl_2 and filtering the resulting suspension through Celite. The resulting clear yellow solution is evaporated to dryness, yielding **2a** as a yellow solid with a 55% yield.

The IR spectrum of **2a** shows the C-O and the C-F stretching vibrations at 1627 cm^{-1} and at 1139 cm^{-1}, respectively, showing the presence of the anionic CF_3CO_2 ligand. The ^1H NMR spectrum shows the disappearance of the signal assigned to H4 in the 5-thiazole fragment, while the signals assigned to the vinyl hydrogen and the phenyl ring remain unchanged, indicating that metallation has selectively occurred on the thiazole ring. These data suggest that the oxazolone coordinates as a C^N-chelating ligand and that the coordination sphere of Pd is completed with the trifluoroacetate group. Due to this, and considering the behavior observed in other structurally related oxazolones, the formation of **2a** is proposed as a dinuclear complex with the carboxylate ligands acting as *O*,*O*′-bridges. Furthermore, the relative arrangement of the two oxazolone chelate fragments must be *transoid*, as inferred from the observation of a single singlet in the ^{19}F NMR spectrum of **2a**, corresponding to the two chemically equivalent CF_3 fragments, as shown in Scheme 1.

Similarly, the reactivity of oxazolones **1b** and **1c** with $Pd(OAc)_2$ in CF_3CO_2H was tested under a variety of conditions. All attempts to obtain an orthometalated product from oxazolone **1c** were unsuccessful, with its decomposition being observed in both trifluoroacetic acid and acetic acid, even at room temperature. The reactivity of **1b** with $Pd(OAc)_2$ was more successful, although the result was surprising. Thus, treatment of **1b** with $Pd(OAc)_2$ (1:1 molar ratio) in CF_3CO_2H at 70 °C for 2 h led to the formation of a deep red solid, completely insoluble in the usual solvents used for NMR, including DMSO. However, this red solid, when suspended in CD_2Cl_2, reacts with excess pyridine-d_5, causing a color change from red to pale yellow and the almost immediate dissolution of the initial suspension. This behavior is typical of Pd systems that maintain carboxylate or halide bridges and is used to characterize highly insoluble orthometalated systems by transforming them into more soluble ones [15,24–26].

The spectroscopic characterization (^{1}H NMR) of this solution shows a mixture of at least two products (see Supplementary Materials) with the same signal pattern but different chemical shifts. The ^{1}H NMR spectrum shows peaks that suggest the presence of a C_6H_4 spin system with two ortho substituents, as well as the presence of the two protons from the thiazole group. Both findings indicate that in oxazolone **1b**, the C-H activation has occurred on the C_6H_5 ring and not on the heterocycle as in the case of **1a**. Incidentally, the activation of C-H bonds in the 4-arylidene ring is much more common than in the 2-aryl ring; therefore, this compound represents a quite rare example of alternative C-H activation in oxazolones [36–39]. The moderate solubility of this compound, even in CD_2Cl_2, prevented the acquisition of high-quality ^{13}C spectra, making it impossible to advance the structural characterization beyond this observation. However, the slow evaporation of these solutions in CD_2Cl_2 led to the formation of a small number of yellow crystals. The resolution of the crystal structure by X-ray diffraction of these crystals did provide relevant information about the course of the reaction.

The structural determination shows that the crystals result from the co-crystallization of an orthopalladated unit (shown in Figure 6) together with the complex $[Pd(py)_4](CF_3CO_2)_2$, and that they also contain CH_2Cl_2. This mixture of palladium complexes crystallizes in the triclinic system, space group P-1, and the asymmetric unit of each unit cell contains one orthometalated complex unit, half of a $[Pd(py)_4]^{2+}$ complex, one CF_3CO_2 anion, and 0.4 molecules of dichloromethane. Various ORTEP diagrams of the contents of the asymmetric unit are shown in the Supplementary Materials, while Figure 6 shows an ORTEP diagram of the complex derived from the orthopalladation of oxazolone **1b**.

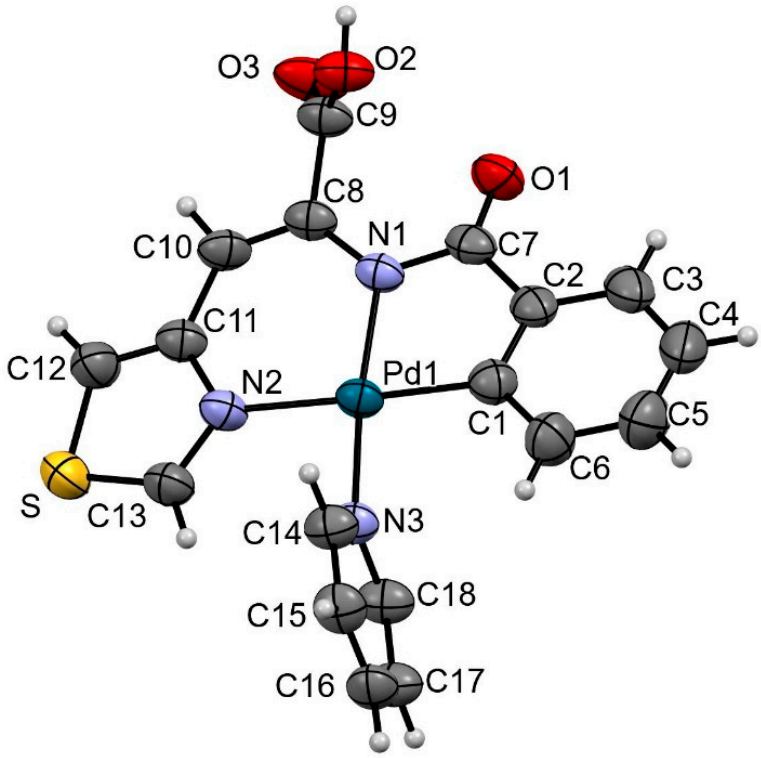

Figure 6. Molecular structure of palladacycle **2b**. Thermal ellipsoids are drawn at 50% probability level.

Figure 6 confirms that, indeed, the C-H activation has occurred at the ortho position of the 2-phenyl ring, while the thiazole group has not undergone any activation of bonds and is simply N-coordinated to the Pd atom. It also shows that the oxazolone ring has undergone a significant modification, as it has been transformed into a N-benzoyl-dehydroamino acid by the opening of the oxazolone ring through hydrolysis and the generation of the carboxylic acid groups C8-C9(O3)O2-H and benzamide N1-C7(O1)-(C1-C6). In addition to the σ(Pd1-C1) bond that formally is anionic and saturates charge, deprotonation of the

benzamide-type N1 has occurred, generating an amide anion that also saturates charge. The coordination of N2 of the thiazole ring causes the dehydroamino acid ligand generated from the oxazolone to act as a κ^3-*N*,*N*,*C*-tridentate ligand. The coordination sphere of Pd is completed by the coordination of a pyridine ligand through nitrogen N3. Beyond the significant transformation that the original oxazolone **1b** has undergone to become the tridentate ligand shown in Figure 6, the analysis of bond distances and angles in this complex and in the co-crystallized species $[Pd(py)_4](CF_3CO_2)_2$ does not show significant deviations from the values found in the literature for related species [40].

According to these results, we propose that the formation of **2b** takes place following the process shown in Scheme 2.

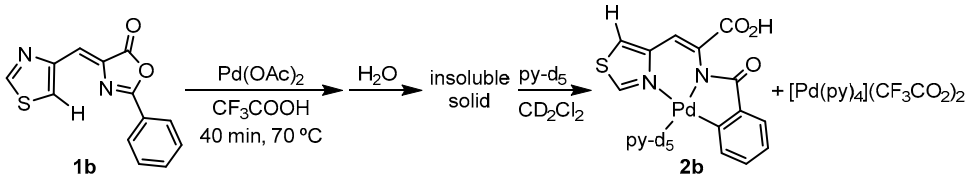

Scheme 2. Alternative C-H activation of oxazolone **1b** and synthesis of **2b**.

Clearly, it is necessary to consider that this characterization corresponds to only a portion of the original sample, as this is only one of the ortho-metalated complexes obtained from the crude compound. Currently, we are focusing on the characterization of the insoluble material.

Regarding the process that leads to the formation of the ortho-metalated complex, the source of the water involved in the hydrolysis reaction and ring-opening could be that contained in the trifluoroacetic acid (the reaction solvent), so the insoluble solid might already contain the hydrolyzed oxazolone ring, or it could be that it was added later for washing. On the other hand, it has not been possible to determine unequivocally whether the C-H activation and ortho-palladation occur after the opening of the oxazolone, that is, in the dehydroamino acid species, or before the opening, in which case it would be an attempt by the system to achieve additional stabilization. Additional control experiments show that it is more plausible to be the latter case, as attempts to orthopalladate the corresponding dehydroamino acid lead to the recovery of the starting products. Similarly, we have observed that in 2 + 2 photodimerization reactions of oxazolones to form cyclobutanes, the opening of the heterocycle and the formation of the corresponding amide esters is a common occurrence, which significantly stabilizes the final cyclobutanes by removing the strain in the oxazolone ring [41]. Therefore, we propose initial C-H activation on the oxazolone, formation of the orthopalladated tridentate complex, and finally, hydrolysis of the oxazolone ring to give the metalated species shown in Figure 6 and Scheme 2.

The differing reactivity of **1a** and **1b** towards $Pd(OAc)_2$, despite their structural similarities, is striking. Our proposal is that the different coordinating abilities of the heteroatoms in the thiazole ring (S vs. N) with respect to palladium could be responsible for this switch in reactivity towards the 2-phenyl ring. In the case of oxazolone **1a**, coordination of the sulfur atom of the thiazole could occur as an alternative to C-H activation. However, sulfur coordination to Pd is inherently weak, and under reaction conditions (70 °C), the Pd-S bond would be very unstable. This could lead to rotation of the thiazole and eventual activation of the C-H bond at position 4 of the thiazole, generating **2a**. In contrast, in oxazolone **1b**, coordination of the nitrogen can occur and may compete with the activation of the bond at position 5 of the thiazole. Furthermore, after coordination of both the nitrogen of the thiazole and the nitrogen of the oxazolone, a stable chelate is formed, which strongly directs C-H activation to the ortho position of the 2-phenyl ring and ultimately leads to the observed ortho-palladation. We do not have a clear explanation for the lack of reactivity of oxazolone **1c**, beyond the fact that the presence of the strongly electron-withdrawing MeC(O) group on the nitrogen of the imidazole may deactivate this ring.

*2.3. Reactivity of (***2a***), Synthesis of* **3a**–**5a**

In order to obtain a greater variety of Pd complexes with ortho-metalated oxazolone **1a** for measuring their photophysical properties, the reactivity of **2a** has been tested in ligand metathesis and bridge cleavage reactions. Dimers with chloride bridges are highly reactive and suitable for preparing a wide range of mononuclear complexes by adding ligands that can act as chelates or nucleophiles to break the chloride bridges. The synthesis of dimer **3a** is carried out from **2a** and the excess of LiCl through a metathesis process where trifluoroacetate bridges are replaced by chloride bridges, as described in the literature and represented in Scheme 3 [24].

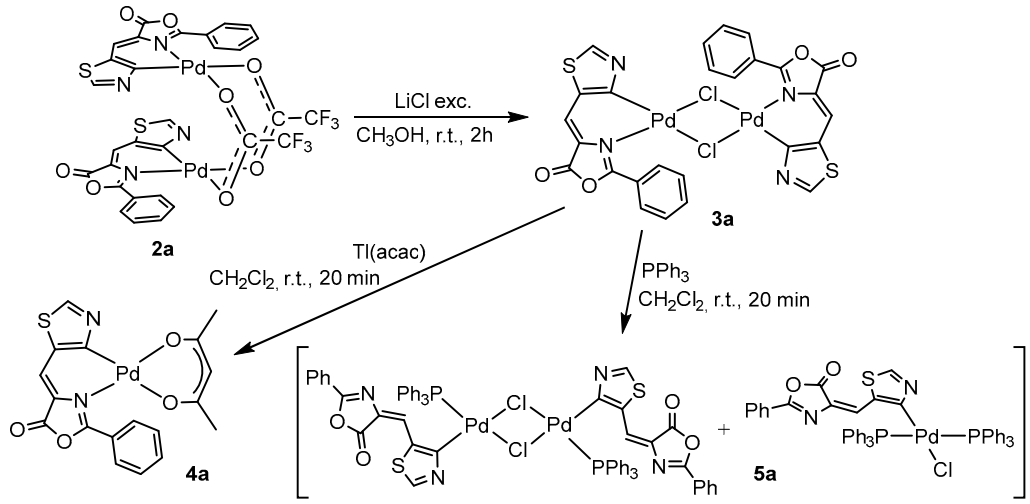

Scheme 3. Synthesis of complexes **3a**–**5a** from **2a**.

Dimer **3a** is obtained as a brown solid, stable to air and moisture, with a yield of 50%, and is insoluble in common solvents used for NMR characterization. The IR spectrum of **3a** shows a clear absorption at 343 cm^{-1}, assigned to the stretching ν(Pd-Cl), as well as the disappearance of the absorptions assigned to the CF_3CO_2 ligand in **2a** (1627 cm^{-1} and 1139 cm^{-1}). On the other hand, the HRMS spectrum of **3a** shows a peak at 758.8235 amu, with an isotopic distribution that is in very good agreement with the stoichiometry $[Pd_2ClC_{26}H_{14}N_4O_4S_2]^+$ (758.8219 amu). These observations indicate the metathesis of carboxylate bridges by chloride and the formation of **3a**.

Treatment of **3a** with Tl(acac) (molar ratio 1:2; acac = acetylacetonate) results in the substitution of the chloride ligands with the chelating acac anion, forming the yellow complex **4a** with an 80% yield, as shown in Scheme 3 [24,42]. Elemental analyses of **4a** are consistent with the stoichiometry proposed in Scheme 3. The ^1H NMR spectrum confirms the incorporation of the acac ligand as an *O*,*O*′-chelate by observing two resonances at 2.06 and 2.04 ppm (relative intensity 3) assigned to the methyl groups, reflecting the asymmetry of the orthopalladated oxazolone ligand, along with a singlet at 5.55 ppm (relative intensity 1) due to the proton of the CH group [42]. The ^{13}C NMR spectrum confirms this asymmetry of the *O*,*O*′-acac ligand, as two resonances are observed for the carbonyl groups (188.06 ppm and 185.8 ppm), as well as for the methyl groups (27.36 ppm and 26.61 ppm), while carbon C3 appears at 100.83 ppm in a typical position for the O,O′-chelated ligand [42].

Finally, the cleavage of the chloride bridge system in **3a** with neutral monodentate ligands has been tested. Treatment of a suspension of **3a** in CH_2Cl_2 with PPh_3 (molar ratio 1:2) results in its immediate dissolution, turning the initial brown suspension into a pale-yellow solution. Removal of the solvent yields a solid **5a**, whose ^{31}P spectrum (see Supplementary Materials) shows the presence of two signals (28.64 ppm and 23.24 ppm), suggesting the formation of two different species. In this case, we can rule out the formation of coordination isomers (PPh_3-trans-N and PPh_3-trans-C), as the reluctance of the PPh_3 ligand to coordinate trans to an aromatic C due to the antisymbiotic effect is well estab-

lished [43]. In closely related works [44], it has been observed that phosphine coordination causes the decoordination of the N atom from the oxazolone, even while maintaining the dinuclear structure. Therefore, it cannot be ruled out that a similar phenomenon is occurring in this case, that is, the coordination of the phosphine and decoordination of the N atom in the dinuclear system, followed by the subsequent rupture with additional phosphine to generate mononuclear systems with two phosphines. By comparing the ^{31}P NMR chemical shifts obtained here with those reported in previous studies, our structural proposal for **5a** is that the obtained mixture corresponds to what is shown in Scheme 3, a dinuclear complex with chloride bridges, an η^1-monodentate oxazolone and a phosphine per Pd, and a mononuclear complex with an η^1-monodentate oxazolone and two *trans* phosphines per Pd [44].

2.4. Photophysical Properties

The optical properties of oxazolones **1a**–**1c** and complexes **2a** and **4a** were measured in CH_2Cl_2 solution (10^{-5} M) at 25 °C. The absorption maxima of the oxazolones and their orthopalladated derivatives are listed in Table 1, and the spectra are shown in the Supplementary Materials. The emission spectra, also shown in the Supplementary Materials, were measured using the absorption maxima observed in the UV-visible spectra. Oxazolones **1a**–**1c** have their maximum (373–386 nm) in the UV A-region, while orthopalladated complexes **2a** and **4a** exhibit their absorbance maximum shifted toward longer wavelengths, in the range of 406–449 nm, corresponding to the blue-ultraviolet region of the UV-Vis spectrum. The presence of absorption bands in this region has been reported for other oxazolones and is attributed to π-π* charge transfer [24,25]. The general bathochromic shift of the absorption maxima from the free ligand to the organometallic complexes has been observed for other palladium-oxazolone complexes and can be interpreted as the palladium contribution to the frontier orbitals. In the case of complex **2a**, two relative absorption maxima are observed, which, as will be discussed later, lead to the same emission.

Table 1. Wavelength values of absorption, excitation and emission maxima (nm).

Compound	$\lambda_{abs.max}$ (nm)	$\lambda_{exc.max}$ (nm)	$\lambda_{emis.max}$ (nm)
1a	378	378	434
1b	386		
1c	373		
2a	425, 449	451	474
4a	406	420	512

Excitation of the compounds at the absorption maxima listed in Table 1 for oxazolone **1a** and complexes **2a** and **4a** results in blue-green emissions (Table 1 and Supplementary Materials). The emission of the complexes is red-shifted compared to that of the free ligand, an effect observed in other palladium complexes with oxazolones [24]. In complex **4a**, a larger Stokes shift is observed, probably reflecting a greater distortion of the molecule in the excited state compared to the ground state. The excitation spectra, recorded at the emission maximum, are consistent with the absorption spectra. Finally, the comparison of the quantum yields measured for **1a** and **2a**, which are both less than 1%, does not allow us to conclude that the presence of the Pd promotes any amplification in this case, as it was observed in other systems [25,26].

3. Materials and Methods

Solvents were obtained from commercial sources and were used without further purification. All reactions were performed without special precautions against air and moisture.

3.1. Synthesis and Characterization of Oxazolones from Heterocycles

The oxazolones **1a**–**1c** were prepared using the Erlenmeyer–Plöchl method, by reaction of the corresponding hippuric acids and aldehydes in acetic anhydride [27–33].

Synthesis of (Z)-4-(5-thiazolylmethylene)-2-phenyl-5(4H)-oxazolone **1a**

In a 50 mL round-bottom flask equipped with a reflux system, thiazole-5-carboxaldehyde (1.000 g, 8.57 mmol), hippuric acid (1.567 g, 8.57 mmol), and sodium acetate (0.700 g, 8.57 mmol) were dissolved in acetic anhydride (10 mL, 106.46 mmol). The resulting mixture was heated in an oil bath at 100 °C with stirring for 2 h. After the reaction time, the heating plate was turned off, and the mixture was allowed to cool, resulting in a precipitated solid containing impure oxazolone **1a**. This precipitate was treated with 10 mL of ethanol and stirred for 5 min at room temperature. The insoluble solid was then collected on a filter plate, washed twice with ethanol (2 × 10 mL), and twice with distilled water (2 × 10 mL). The resulting yellow solid was dried under suction and characterized as oxazolone **1a**. Obtained: 2.13 g (yield: 97%). ^{1}H NMR ($CDCl_3$, 400.13 MHz, 298 K): δ = 9.05 (dd, 1H, H_2, thiazole), 8.32 (dd, 1H, H_4, thiazole), 8.18 (m, 2H, H_o, Ph), 7.64 (tt, 1H, H_p, Ph, $^{3}J_{HH}$ = 7.2 Hz, $^{4}J_{HH}$ = 2.4 Hz), 7.55 (m, 2H, H_m, Ph), 7.53 (dd, 1H, H vinyl). ^{13}C NMR ($CDCl_3$, 100.67 MHz, 298 K): δ = 165.82 (C=O), 163.47 (C=N), 159.62 (C_2 thiazole), 149.26 (C_4, thiazole), 133.57 (C_p, Ph), 133.22 (=C), 132.38 (C_5, thiazole), 128.89 (C_m, Ph), 128.38 (C_o, Ph), 125.02 (C_i, Ph), 120.97 (=CH, vinyl). HRMS (ESI$^+$) [m/z]: calculated for $[C_{13}H_8N_2O_2S+K]^+$ =294.9944; found 294.9967.

Synthesis of (Z)-4-(4-thiazolylmethylene)-2-phenyl-5(4H)-oxazolone **1b**

Oxazolone **1b** is prepared following the same experimental procedure described for **1a** but using the corresponding aldehyde. Thus, thiazole-4-carbaldehyde (0.500 g, 4.29 mmol), hippuric acid (0.784 g, 4.29 mmol), and sodium acetate (0.350 g, 4.29 mmol) reacted with acetic anhydride (5 mL, 53.23 mmol) under reflux (100 °C, 2 h) to yield oxazolone **1b** as a yellow solid after washing with ethanol (2 × 10 mL) and water (2 × 10 mL). Obtained: 0.43 g (yield: 39%). ^{1}H NMR ($CDCl_3$, 500.13 MHz, 298 K): δ = 8.88 (d, 1H, H_2, thiazole, $^{4}J_{HH}$ = 2 Hz), 8.81 (d, 1H, H_5, thiazole, $^{4}J_{HH}$ = 2 Hz), 8.17 (m, 2H, H_o, Ph), 7.62 (tt, 1H, H_p, Ph, $^{3}J_{HH}$ = 7.5 Hz, $^{4}J_{HH}$ = 1.5 Hz), 7.56 (s, 1H, H vinyl), 7.53 (m, 2H, H_m, Ph). ^{13}C NMR ($CDCl_3$, 125.67 MHz, 298 K): δ = 166.58 (C=O), 164.29 (C=N), 152.43 (C_2, thiazole), 150.64 (C_4, thiazole), 134.06 (=C), 133.56 (C_p, Ph), 128.39 (C_o, Ph), 128.88 (C_m, Ph),126.07 (C_5, thiazole), 125.19 (C_i, Ph), 123.81 (=CH, vinyl). HRMS (ESI$^+$) [m/z]: calculated for $[C_{13}H_8N_2O_2S+K]^+$ = 294.9944; found 294.9982.

Synthesis of (Z)-4-(4-(1-acetyl-1H-imidazolylmethylene)-2-phenyl-5(4H)-oxazolone **1c**

Oxazolone **1c** is prepared following the same experimental procedure described for **1a** but using the corresponding aldehyde. Thus, imidazole-4-carbaldehyde (0.500 g, 5.10 mmol), hippuric acid (0.932 g, 5.10 mmol), and sodium acetate (0.420 g, 5.10 mmol) reacted with acetic anhydride (5 mL, 53.23 mmol) under reflux (100 °C, 2 h) to yield oxazolone **1c** as a yellow solid after washing with ethanol (2 × 10 mL) and water (2 × 10 mL). Obtained: 0.81 g (yield: 75%). ^{1}H NMR ($CDCl_3$, 400.13 MHz, 298 K): δ = 8.54 (dd, 1H, H_2, imidazole, $^{4}J_{HH}$ = 1.6 Hz, $^{5}J_{HH}$ = 0.8 Hz), 8.21 (d, 1H, H_5, imidazole, $^{4}J_{HH}$ = 1.2 Hz), 8.14 (m, 2H, H_o, Ph), 7.61 (tt, 1H, H_p, Ph, $^{3}J_{HH}$ = 8 Hz, $^{4}J_{HH}$ = 2 Hz), 7.52 (m, 2H, H_m, Ph), 7.29 (d, 1H, H vinyl, $^{5}J_{HH}$ = 0.4 Hz), 2.70 (s, 3H, CH_3, acetyl). ^{13}C NMR ($CDCl_3$, 100.67 MHz, 298 K): δ = 166.13 (C=O, oxazolone), 165.88 (C=O, acetyl), 163.46 (C=N), 138.27 (C_4, imidazole), 136.72 (C_5, imidazole), 133.29 (C_p, Ph), 133.28 (=C), 128.80 (C_m, Ph), 128.25 (C_o, Ph), 125.12 (C_i, Ph), 123.37 (=CH, vinyl), 121.52 (C_2, imidazole), 22.70 (CH_3, acetyl). HRMS (ESI$^+$) [m/z]: calculated for $[C_{15}H_{11}N_3O_3 + Na]^+$ = 304.0698; found 304.0691.

3.2. Synthesis of Orthopalladated Derivatives **2a**–**5a** and **2b**

The incorporation of the palladium to the oxazolone ligand through C-H bond activation has been carried out in refluxing trifluoroacetic acid, following the methods previously reported [24–26,36–39].

Synthesis of orthopalladated complex **2a**

A suspension of $Pd(OAc)_2$ (0.663 g, 2.93 mmol) and **1a** (0.750 g, 2.93 mmol) in CF_3CO_2H (15 mL) was heated to 70 °C in an oil bath with stirring for 40 min. After the reaction time, the system was allowed to reach room temperature, resulting in the formation of a black suspension. To this suspension, 15 mL of distilled water was added, causing an increase in the precipitated solid. The mixture was stirred at room temperature for 5 min. The black precipitated solid was filtered, washed with 3 portions of distilled water (3 × 10 mL), dried under suction, and characterized as compound **2a** contaminated with black palladium. To recrystallize **2a**, the black solid was treated with CH_2Cl_2 (about 75 mL), stirred at room temperature for 10 min, and the resulting suspension was filtered through Celite, washing the Celite until the washings were colorless (about 25 mL additional). The resulting intense yellow solution was evaporated to dryness, yielding **2a** as an intense yellow solid. Obtained: 1.513 g (yield: 55%). ^{1}H NMR (CD_2Cl_2, 500.13 MHz, 298 K): δ = 8.89 (s, 1H, H_2 thiazole), 8.53 (m, 2H, H_o, Ph), 7.76 (tt, 1H, H_p, Ph, $^3J_{HH}$ = 7.5 Hz, $^4J_{HH}$ = 1 Hz), 7.66–7.63 (m, 3H, H_m Ph + H vinyl). ^{13}C NMR (CD_2Cl_2, 125.67 MHz, 298 K): δ = 170.57 (C=N), 164.50 (C=O), 160.01 (C_2, thiazole), 156.7 (Pd-C_4, thiazole), 135.95 (C_p, Ph), 131.39 (C_o, Ph), 128.87 (C_m, Ph), 125.03 (=CH, vinyl), 123.46 (C_5, thiazole), 122.21 (Ci, Ph). The compound has a low solubility, even in CD_2Cl_2, and the spectra were acquired in long trials using a saturated solution. Despite this, signals due to the quaternary C atoms (=C, C-O and C-F) could not be found in the ^{13}C spectrum due to the low S/N ratio, neither through correlations in the HMBC spectrum. ^{19}F NMR ($CDCl_3$, 470.55 MHz, 298 K): δ = −76.27 (s, CF_3). IR (ν, cm^{-1}): 1799 (C=O), 1660, 1571 (O-C=N), 1627 (C-O bridging), 1139 (C-F). Elemental Analysis. Found: C, 38.07; H, 1.40; N, 5.78; S, 6.51. Calculated for $C_{30}H_{14}F_6N_4O_8Pd_2S_2$: C, 37.95; H, 1.49; N, 5.90; S, 6.75.

Synthesis of orthopalladated complex **3a** *[24]*

A suspension of **2a** (0.600 g, 0.63 mmol) in methanol (25 mL) was treated with anhydrous LiCl (0.107 g, 2.52 mmol), and the mixture was stirred at room temperature for 2 h. After the reaction time, the resulting precipitated solid was filtered and washed with 5 mL of cold methanol and 20 mL of diethyl ether. The brown product was dried by suction and characterized as **3a**. Obtained: 0.269 g (yield: 54%). **3a** was found to be completely insoluble in common deuterated solvents, so it could not be characterized by NMR methods. IR (ν, cm^{-1}): 1794 (C=O), 1625 (O-C=N), 343 (Pd-Cl). HRMS (ESI^+) [m/z]: calculated for $[C_{26}H_{14}ClN_4O_4Pd_2S_2]^+ = [M\text{-}Cl]^+$ = 758.8219; found 758.8235.

Synthesis of orthopalladated complex **4a** *[24,42]*

A suspension of **3a** (0.150 g, 0.189 mmol) in CH_2Cl_2 (15 mL) at room temperature was treated with Tl(acac) (0.115 g, 0.378 mmol). The resulting suspension was stirred at room temperature for 20 min. After this time, the precipitated TlCl was removed by filtration through Celite. The Celite was washed with additional CH_2Cl_2 (10 mL) and the combined solutions were evaporated to dryness. The resulting residue was treated with 20 mL of cold *n*-pentane and stirring. The resulting yellow solid (**4a**) was filtered, washed with additional cold *n*-pentane (2 × 5 mL), dried under suction and characterized as **4a**. Obtained: 0.14 g (yield: 80%). ^{1}H NMR ($CDCl_3$, 500.13 MHz, 298 K): δ = 8.99 (d, 1H, H_2, thiazole, $^5J_{HH}$ = 1 Hz), 8.12 (m, 3H, H_o, Ph + H vinyl), 7.58 (tt, 1H, H_p, Ph, $^3J_{HH}$ = 8 Hz, $^4J_{HH}$ = 2 Hz), 7.50 (m, 2H, H_m, Ph), 5.55 (s, 1H, CH, acac), 2.05 (s, 3H, CH_3, acac), 2.03 (s, 3H, CH_3, acac). ^{13}C NMR ($CDCl_3$, 125.67 MHz, 298 K): δ = 188.06 (C-O, acac), 185.80 (C-O, acac), 170.66 (C_4, thiazole), 166.74 (C=O), 161.44 (C=N), 158.42 (C_2, thiazole), 132.92 (C_p, Ph), 130.55 (=C), 129.98 (C_5, thiazole), 128.81 (C_m, Ph), 128.07 (C_o, Ph), 127.86 (=CH, vinilo), 125.60 (C_i, Ph), 100.83 (CH, acac), 27.36 (CH_3, acac), 26.61 (CH_3, acac). Elemental Analysis. Found: C, 46.66; H, 3.37; N, 5.73; S, 7.09. Calculated for $C_{18}H_{14}N_2O_4PdS$: C, 46.92; H, 3.06; N, 6.08; S, 6.96.

Reactivity of **3a** *with* PPh_3 (**5a**)

A suspension of **3a** (0.150 g, 0.19 mmol) in CH_2Cl_2 (15 mL) at room temperature was treated with PPh_3 (0.100 g, 0.38 mmol). The resulting suspension was stirred at room temperature for 20 min, during which time the initial suspension dissolved. After this period, any remaining insoluble solid was removed by filtration. The obtained solution

was evaporated to dryness, and the residue was treated with 20 mL of cold *n*-pentane with stirring. The resulting pale yellow solid was filtered, washed with two additional 5 mL portions of cold *n*-pentane, and dried by suction. The resulting solid was characterized as the mixture **5a** (see text). Obtained: 0.06 g. ^{31}P NMR ($CDCl_3$, 202.46 MHz, 298 K): δ = 28.64 ppm (s, 1P, PPh_3), 23.24 ppm (s, 2P, PPh_3).

Synthesis of orthopalladated complex co-crystallized with [Pdpy$_4$](CF$_3$CO$_2$)$_2$ (**2b**)

A suspension of $Pd(OAc)_2$ (0.137 g, 0.61 mmol) and **1b** (0.157 g, 0.61 mmol) in CF_3CO_2H (10 mL) was heated to 70 °C in an oil bath with stirring for 40 min. After this time, the reaction was cooled to room temperature, resulting in the formation of a deep red suspension. To this suspension, 15 mL of distilled water was added, resulting in an increase in the amount of precipitated solid. The precipitated solid was filtered, washed with additional portions of distilled water (3 × 10 mL), one portion of acetone (10 mL), one portion of CH_2Cl_2 (10 mL), and dried by suction. The solid thus generated (0.130 g) showed to be totally insoluble in the usual deuterated solvents. However, a suspension of this insoluble solid (10 mg) in CD_2Cl_2 (0.6 mL) reacted with 1 drop of py-d_5 producing the instantaneous solution of the initial suspension and the obtention of a clear yellow solution, containing **2b** and other species, which was partially characterized by ^{1}H NMR. Slow evaporation of this solution gave a small crop of crystals of (**2b**), which was characterized as the co-crystallization of [Pd(NˆNˆC)(py)] and $[(Pdpy_4)(CF_3CO_2)_2]_{0.5}(CD_2Cl_2)_{0.8}$.

3.3. Spectroscopic and Analytical Methods

The ^{1}H, ^{13}C and ^{19}F NMR spectra of the isolated products were recorded in $CDCl_3$ or CD_2Cl_2 solutions at 25 °C on Bruker AV300, AV400, or Bruker AV500 spectrometers (δ in ppm, *J* in Hz) at ^{1}H operating frequencies of 300.13, 400.13, and 500.13 MHz, respectively. The ^{1}H and ^{13}C NMR spectra were referenced using the solvent signal as the internal standard, while ^{19}F NMR spectra were referenced to $CFCl_3$. The ^{13}C NMR peaks were identified using standard ^{1}H−^{13}C edited-HSQC and ^{1}H−^{13}C HMBC 2D-experiments. In both cases 4K points in t_2 using spectral widths of 10 ppm (^{1}H) and 200 ppm (^{13}C) were used, with averaged values of the coupling constants $^1J_{CH}$ = 145 Hz and long-range $^nJ_{CH}$ = 10 Hz. Typically, 128 t_1 experiments were recorded and zero-filled to 2K. For each t_1 value 8 (HSQC) or 32 (HMBC) scans were signal-averaged using a recycle delay of 1 s. High-resolution mass spectra-ESI (HRMS-ESI) were recorded using either a Bruker MicroToF-Q™ system equipped with an API-ESI source and a Q-ToF mass analyzer, or a TIMS-TOF system, both allowing a maximum error in the measurement of 5 ppm. Acetonitrile was used as solvent. For all types of MS measurements, samples were introduced in a continuous flow of 0.2 mL/min and nitrogen served both as the nebulizer gas and the dry gas. Absorption spectra were measured on a Thermo Scientific Evolution 600 BB spectrophotometer. The steady-state excitation–emission spectra were measured on a FluoTime300 PicoQuant spectrometer. All measurements were carried out at room temperature on solutions of 10^{-5} M concentration using quartz cuvettes of 1 cm path length. All measurements were carried out at room temperature on solutions of 10^{-5} M concentration using quartz cuvettes of 1 cm path length. Quantum yields of 5×10^{-4} M solutions of **1a** and **2a** in CH_2Cl_2 were measured by the absolute method using a Hamamatsu Quantaurus-QY C11347 compact one-box absolute quantum yield measurement system. Through studies carried out for different substances using both the absolute method and the comparative one, the relative uncertainty for the absolute method has been determined as less than 6% [45].

3.4. X-Ray Crystallography

Crystals of compounds **1c** were obtained by slow diffusion of *n*-pentane into a solution of the crude compound in CH_2Cl_2 at −18 °C over the course of one week, while crystals of **2b** ([Pd(NˆNˆC)(py)] co-crystallized with $[Pd(py)_4](CF_3CO_2)_2$) were obtained by slow evaporation of a CD_2Cl_2 solution containing both compounds (see text). **Data collection.** The selected crystal of **1c** was placed on a micromount coated with protecting perfluoropolyether oil and cooled to 100 K with an open-flow nitrogen gas. X-ray diffrac-

tion data of **1c** was collected at XALOC beamline [46] of Alba-CELLS synchrotron (Spain) (λ = 0.72940 Å) measuring 360 phi scans with two different κ angle values, on a single axis MD2 Maatel diffractometer and a PILATUS 6M detector. Diffraction images were integrated using SAINT [47], and the integrated intensities were scaled and corrected for absorption using SADABS program [48], included in APEX2 package. The selected crystal of **2b** was placed randomly at the end of a glass fiber and covered with perfluorinated oil (magic oil). Data collection was performed at 295 K (**2b**) using an Oxford Diffraction Xcalibur diffractometer with Mo-Kα radiation (graphite monochromator, λ = 0.71073 Å). A hemisphere of data was collected based on scans of ω and φ angles, and the diffraction images were integrated and corrected for absorption using CrysAlis Pro software (https://rigaku.com/products/crystallography/x-ray-diffraction/crysalispro) [49]. **Structure solution and refinement.** The structures were solved using direct methods [50,51]. Refinement of all non-hydrogen atoms was carried out with anisotropic displacement parameters. Hydrogen atoms of **1c** were included in the model in observed positions and freely refined. Hydrogen atoms of **2b** were placed in positions calculated mathematically as riding atoms on the atoms to which they are bonded (C, N, O), except those noted below, and were assigned an isotropic displacement parameter equal to 1.2 or 1.5 times the equivalent isotropic displacement parameter of the bonded atom. The structures were refined with respect to F_o^2, and all reflections were used in the least-squares calculations [51,52]. The resolution of the crystal structure of **2b** shows that the asymmetric part of the unit cell contains one molecule of the orthometalated complex [Pd(NˆNˆC)(py)], half of a $[Pdpy4]^{2+}$, one $(CF_3CO_2)^-$, and 0.4 of dichloromethane. The CF_3 group has a rotational disorder in the F atoms, modeled with occupancies of 0.8/0.2. Constraints are applied to the C-F distances (SAME) and the thermal parameters of the F atoms. The position of the hydrogen atom of the OH fragment is found in the electron density maps. It is refined using a free isotropic parameter with a fixed O-H distance of 0.82 Å. There is a hydrogen bond between this OH group and an oxygen atom of the trifluoroacetate. **CCDC 2384620** (**2b**) and **2384671** (**1c**) contain the supplementary crystallographic data. These data can be obtained free of charge from the Cambridge Crystallographic Data Centre via www.ccdc.cam.ac.uk/structures/.

4. Conclusions

In summary, the synthesis of (*Z*)-4-hetarylidene-5(4*H*)-oxazolones **1** for various heterocycles (thiazole, imidazole) has been carried out, and it has been found that they are not fluorescent species. It has also been demonstrated that the incorporation of Pd by C-H activation into the heterocycle located at the 4-hetarylidene position in various organometallic complexes **2**–**5** does not lead, in these cases, to a clearly detectable fluorescence amplification due to the suppression of the hula-twist deactivation pathway. Unexpectedly, it has been observed in thiazole derivatives that the different location of the vinyl group –C(H)=C (5 vs. 4) relative to the heteroatoms of the thiazole (N, S) affects the position of C-H activation and subsequent orthopalladation. Thus, when the vinyl group is in position 5, the thiazole heterocycle is orthopalladated at position 4, while when the vinyl group is in position 4, N-coordination of the thiazole occurs, and the unprecedented activation of the phenyl ring in position 2 of the oxazolone is produced.

Supplementary Materials: The following supporting information can be downloaded at https://www.mdpi.com/article/10.3390/inorganics12100271/s1. Copies of ^1H and ^{13}C NMR spectra of all new species; UV-VIS Absorption and emission spectra of all new species; Table S1: Crystal data and structure refinement for **1c**; Table S2: Bond distances (Å) and angles (°) for **1c**; Table S3: Crystal data and structure refinement for **2b**; Table S4. Bond distances (Å) and angles (°) for **2b**; ORTEP drawings of the contents of the asymmetric part of the unit cell of **2b**.

Author Contributions: Conceptualization, D.D. and E.P.U.; methodology, D.D. and M.M.; validation, M.M., D.D. and E.P.U.; formal analysis, M.M., D.D., O.C., P.G.-O., F.L. and A.M.; investigation, M.M., D.D., O.C., P.G.-O., F.L. and A.M.; resources, E.P.U.; data curation, M.M., D.D., O.C., P.G.-O., F.L. and A.M.; writing—original draft preparation, M.M. and E.P.U.; writing—review and editing, all authors;

supervision, E.P.U.; project administration, E.P.U.; funding acquisition, E.P.U. All authors have read and agreed to the published version of the manuscript.

Funding: Spanish Government (grants PID2019-106394GB-I00 and PID2022-136861NB-I00, funded by MCIN/AEI/10.13039/501100011033, and grant PID2021-122869NB-I00 funded by MICIU/AEI/10.13039/501100011033 and ERDF/EU.) and Gobierno de Aragón-FSE (Spain, research groups Química Inorgánica y de los Compuestos Organometálicos E17_23R and Química de Oro y Plata E07_23R).

Data Availability Statement: Additional data are contained within the article and Supplementary Materials.

Acknowledgments: E.P.U. and D.D. thank the Spanish Government (grant PID2019-106394GB-I00, funded by MCIN/AEI/10.13039/501100011033); A.M. also thanks the Spanish Government (grant PID2021-122869NB-I00 funded by MICIU/AEI/10.13039/501100011033 and ERDF/EU); E.P.U., A.M. and D.D. thank Gobierno de Aragón-FSE (Spain, research groups Química Inorgánica y de los Compuestos Organometálicos E17_23R) for funding. D. Dalmau thanks Gobierno de Aragón-FSE for a PhD fellowship. Some X-ray diffraction experiments were performed at XALOC beamline at ALBA Synchrotron with the collaboration of ALBA staff.

Conflicts of Interest: The authors declare no conflicts of interest.

References

1. Valeur, B.; Berberan-Santos, M.N. *Molecular Fluorescence, Principles and Applications*, 2nd ed.; Wiley-VCH: Weinheim, Germany, 2013.
2. Edgar, A. Luminescent Materials. In *Springer Handbook of Electronic and Photonic Materials*; Kasap, S., Capper, P., Eds.; Springer Handbooks; Springer: Cham, Switzerland, 2017.
3. Kitai, A. *Luminescent Materials and Applications*, 1st ed.; Wiley-VCH: Weinheim, Germany, 2008.
4. Kandarakis, I.S. Luminescence in medical image science. *J. Lumin.* **2016**, *169*, 553–558. [CrossRef]
5. Ronda, C. Challenges in Application of Luminescent Materials, a Tutorial Overview. *Prog. Electromagn. Res.* **2014**, *147*, 81–93. [CrossRef]
6. Prodi, L.; Montalti, M.; Zaccheroni, N. Luminescence Applied in Sensor Science. *Top. Curr. Chem.* **2011**, *300*, 1–217.
7. Feldmann, C.; Jüstel, T.; Ronda, C.R.; Schmidt, P.J. Inorganic Luminescent Materials: 100 Years of Research and Application. *Adv. Funct. Mater.* **2003**, *13*, 511–516. [CrossRef]
8. Shimomura, O. Discovery of green fluorescent protein (GFP) (Nobel Lecture). *Angew. Chem. Int. Ed.* **2009**, *48*, 5590–5602. [CrossRef]
9. Chalfie, M. GFP: Lighting Up Life (Nobel Lecture). *Angew. Chem. Int. Ed.* **2009**, *48*, 5603–5611. [CrossRef]
10. Tsien, R.Y. Constructing and Exploiting the Fluorescent Protein Paintbox (Nobel Lecture). *Angew. Chem. Int. Ed.* **2009**, *48*, 5612–5626. [CrossRef]
11. Remington, S.J. Fluorescent proteins: Maturation, photochemistry and photophysics. *Curr. Opin. Struct. Biol.* **2006**, *16*, 714–721. [CrossRef]
12. Pakhomov, A.A.; Martynov, V.I. GFP Family: Structural Insights into Spectral Tuning. *Chem. Biol.* **2008**, *15*, 755–764. [CrossRef]
13. Wachter, R.M. Chromogenic Cross-Link Formation in Green Fluorescent Protein. *Acc. Chem. Res.* **2007**, *40*, 120–127. [CrossRef]
14. Mizuno, H.; Mal, T.K.; Tong, K.I.; Ando, R.; Furuta, T.; Ikura, M.; Miyawaki, A. Photo-Induced Peptide Cleavage in the Green-to-Red Conversion of a Fluorescent Protein. *Mol. Cell.* **2003**, *12*, 1051–1058.
15. Collado, S.; Pueyo, A.; Baudequin, C.; Bischoff, L.; Jiménez, A.I.; Cativiela, C.; Hourau, C.; Urriolabeitia, E.P. Orthopalladation of GFP-Like Fluorophores Through C–H Bond Activation: Scope and Photophysical Properties. *Eur. J. Org. Chem.* **2018**, *2018*, 6158–6166. [CrossRef]
16. Ivashkin, P.E.; Yampolsky, I.V.; Lukyanov, K.A. Synthesis and properties of chromophores of fluorescent proteins. *Russ. J. Bioorg. Chem.* **2009**, *35*, 652–669. [CrossRef] [PubMed]
17. Follenius-Wund, A.; Bourotte, M.; Schmitt, M.; Iyice, F.; Lami, H.; Bourguignon, J.J.; Haiech, J.; Pigault, C. Fluorescent derivatives of the GFP chromophore give a new insight into the GFP fluorescence process. *Biophys. J.* **2003**, *85*, 1839–1850.
18. Rajbongshi, B.K.; Sen, P.; Ramanathan, G. Twisted intramolecular charge transfer in a model green fluorescent protein luminophore analog. *Chem. Phys. Lett.* **2010**, *494*, 295–300. [CrossRef]
19. Martin, M.E.; Negri, F.; Olivucci, M. Origin, Nature, and Fate of the Fluorescent State of the Green Fluorescent Protein Chromophore at the CASPT2//CASSCF Resolution. *J. Am. Chem. Soc.* **2004**, *126*, 5452–5464. [CrossRef]
20. Altoe', P.; Bernardi, F.; Garavelli, M.; Orlandi, G.; Negri, F. Solvent effects on the vibrational activity and photodynamics of the green fluorescent protein chromophore: A quantum-chemical study. *J. Am. Chem. Soc.* **2005**, *127*, 3952–3963. [CrossRef]
21. Megley, C.M.; Dickson, L.A.; Maddalo, S.L.; Chandler, G.J.; Zimmer, M. Photophysics and dihedral freedom of the chromophore in yellow, blue, and green fluorescent protein. *J. Phys. Chem. B* **2009**, *113*, 302–308. [CrossRef]
22. Wu, L.; Burgess, K. Syntheses of Highly Fluorescent GFP-Chromophore Analogues. *J. Am. Chem. Soc.* **2008**, *130*, 4089–4096. [CrossRef]

23. Baranov, M.S.; Lukyanov, K.A.; Borissova, A.O.; Shamir, J.; Kosenkov, D.; Slipchenko, L.V.; Tolbert, L.M.; Yampolsky, I.V.; Solntsev, K.M. Conformationally Locked Chromophores as Models of Excited-State Proton Transfer in Fluorescent Proteins. *J. Am. Chem. Soc.* **2012**, *134*, 6025–6032. [CrossRef]
24. Laga, E.; Dalmau, D.; Arregui, S.; Crespo, O.; Jiménez, A.I.; Pop, A.; Silvestru, C.; Urriolabeitia, E.P. Fluorescent Orthopalladated Complexes of 4-Aryliden-5(4*H*)-oxazolones from the Kaede Protein: Synthesis and Characterization. *Molecules* **2021**, *26*, 1238. [CrossRef] [PubMed]
25. Dalmau, D.; Crespo, O.; Matxain, J.M.; Urriolabeitia, E.P. Fluorescence Amplification of Unsaturated Oxazolones Using Palladium: Photophysical and Computational Studies. *Inorg. Chem.* **2023**, *62*, 9792–9806. [CrossRef] [PubMed]
26. Dumitras, D.; Dalmau, D.; García-Orduña, P.; Pop, A.; Silvestru, A.; Urriolabeitia, E.P. Orthopalladated imidazolones and thiazolones: Synthesis, photophysical properties and photochemical reactivity. *Dalton Trans.* **2024**, *53*, 8948–8967. [CrossRef] [PubMed]
27. Erlenmeyer, E. Ueber die Condensation der Hippursäure mit Phtalsäureanhydrid und mit Benzaldehyd. *Justus Liebigs Ann. Der Chem.* **1893**, *275*, 1–8.
28. Plöchl, J. Ueber Phenylglycidasäure (Phenyloxacrylsäure). *Chem. Ber.* **1883**, *16*, 2815. [CrossRef]
29. Plöchl, J. Ueber einige Derivate der Benzoylimidozimmtsäure. *Chem. Ber.* **1884**, *17*, 1616. [CrossRef]
30. Carter, H.E. Azlactones. *Org. React.* **1946**, *3*, 198–237.
31. Filler, R. *Advances in Heterocyclic Chemistry*; Katritzky, A.R., Ed.; Academic Press: New York, NY, USA, 1954; Volume 4, p. 75.
32. Rao, Y.S.; Filler, R. Geometric Isomers of 2-Aryl(Aralkyl)-4-arylidene(alkylidene)-5(4H)-oxazolones. *Synthesis* **1975**, *12*, 749–764. [CrossRef]
33. Rao, Y.S.; Filler, R. Oxazoles. In *The Chemistry of Heterocyclic Compounds*; Turchi, I.J., Ed.; John Wiley & Sons, Inc.: New York, NY, USA, 1986; Volume 3, pp. 363–691.
34. Prokof'ev, E.P.; Karpeiskaya, E.I. The Proton Coupled ^{13}C NMR Direct Determination of *Z*-, *E*-Configuration of 4-Benzyliden-2-Phenyl(Methyl)- Δ^2-Oxazolin-5-Ones and Products of Their Solvolysis. *Tetrahedron Lett.* **1979**, *20*, 737–740. [CrossRef]
35. Vogeli, U.; von Phillipsborn, W. Vicinal C,H Spin Coupling in Substituted Alkenes. Stereochemical Significance and Structural Effects. *Org. Magn. Reson.* **1975**, *7*, 617–627. [CrossRef]
36. Roiban, G.D.; Serrano, E.; Soler, T.; Aullón, G.; Grosu, I.; Cativiela, C.; Martínez, M.; Urriolabeitia, E.P. Regioselective Orthopalladation of (Z)-2-Aryl-4-Arylidene-5(4H)-Oxazolones: Scope, Kinetico-Mechanistic, and Density Functional Theory Studies of the C–H Bond Activation. *Inorg. Chem.* **2011**, *50*, 8132–8143. [CrossRef] [PubMed]
37. Roiban, D.; Serrano, E.; Soler, T.; Grosu, I.; Cativiela, C.; Urriolabeitia, E.P. Unexpected [2 + 2] C–C bond coupling due to photocycloaddition on orthopalladated (*Z*)-2-aryl-4-arylidene-5(4*H*)-oxazolones. *Chem. Commun.* **2009**, 4681–4683. [CrossRef] [PubMed]
38. Serrano, E.; Juan, A.; García-Montero, A.; Soler, T.; Jiménez-Márquez, F.; Cativiela, C.; Gomez, M.V.; Urriolabeitia, E.P. Stereoselective Synthesis of 1,3-Diaminotruxillic Acid Derivatives: An Advantageous Combination of C–H–ortho–Palladation and On-Flow [2 + 2]–Photocycloaddition in Microreactors. *Chem. Eur. J.* **2016**, *22*, 144–152. [CrossRef] [PubMed]
39. Carrera, C.; Denisi, A.; Cativiela, C.; Urriolabeitia, E.P. Functionalized 1,3-Diaminotruxillic Acids by Pd-Mediated C–H Activation and [2 + 2]–Photocycloaddition of 5(4*H*)–Oxazolones. *Eur. J. Inorg. Chem.* **2019**, *2019*, 3481–3489. [CrossRef]
40. Guy Orpen, A.; Brammer, L.; Allen, F.H.; Kennard, O.; Watson, D.G.; Taylor, R. Supplement. Tables of bond lengths determined by X-ray and neutron diffraction. Part 2. Organometallic compounds and co-ordination complexes of the d- and f-block metals. *J. Chem. Soc. Dalton Trans.* **1989**, S1–S83.
41. Sierra, S.; Gomez, M.V.; Jiménez, A.I.; Pop, A.; Silvestru, C.; Marín, M.L.; Boscá, F.; Sastre, G.; Gómez-Bengoa, E.; Urriolabeitia, E.P. Stereoselective, Ruthenium-Photocatalyzed Synthesis of 1,2-Diaminotruxinic Bis-amino Acids from 4-Arylidene-5(4*H*)-oxazolones. *J. Org. Chem.* **2022**, *87*, 3529–3545. [CrossRef]
42. Forniés, J.; Martínez, F.; Navarro, R.; Urriolabeitia, E.P. Synthesis and reactivity of acetylacetonato-Cγ complexes of M^{II} (M = Pd or Pt): X-ray crystal structure of [Pd(C_6F_5)(OOCPh)(bipy)]. *J. Organomet. Chem.* **1995**, *495*, 185–194. [CrossRef]
43. Pearson, R. Antisymbiosis and the trans effect. *Inorg. Chem.* **1973**, *12*, 712–713. [CrossRef]
44. Roiban, D.; Serrano, E.; Soler, T.; Contel, M.; Grosu, I.; Cativiela, C.; Urriolabeitia, E.P. Ortho-Palladation of (*Z*)-2-Aryl-4-Arylidene-5(4*H*)-Oxazolones. Structure and Functionalization. *Organometallics.* **2010**, *29*, 1428–1435. [CrossRef]
45. Würth, C.; Grabolle, M.; Pauli, J.; Spieles, M.; Resch-Genger, U. Comparison of Methods and Achievable Uncertainties for the Relative and Absolute measurement of Photoluminescence Quantum Yields. *Anal. Chem.* **2011**, *83*, 3431–3439. [CrossRef]
46. Juanhuix, J.; Gil-Ortiz, F.; Cuní, G.; Colldelram, C.; Nicolás, J.; Lidón, J.; Boter, E.; Ruget, C.; Ferrer, S.; Benach, J. Developments in optics and performance at BL13-XALOC, the macromolecular crystallography beamline at the Alba synchrotron. *J. Synchr. Rad.* **2014**, *21*, 679–689. [CrossRef] [PubMed]
47. *SAINT Software Reference Manuals, Version V8.40B in APEX4*; Bruker Analytical Xray Systems, Inc.: Madison, WI, USA, 2016.
48. Krause, L.; Herbst-Irmer, R.; Sheldrick, G.M.; Stalke, D.J. SADABS 2016/2. *Appl. Cryst.* **2015**, *48*, 3–10. [CrossRef] [PubMed]
49. *CrysAlis RED, CCD Camera Data Reduction Program*; Rigaku Oxford Diffraction: Oxford, UK, 2019.
50. Sheldrick, G.M. SHELXS-86, Phase annealing in SHELX-90: Direct methods for larger structures. *Acta Crystallogr.* **1990**, *A46*, 467. [CrossRef]

51. Sheldrick, G.M. *SHELXS 97 and SHELXL 97, Program for Crystal Structure Solution and Refinement*; University of Göttingen: Göttingen, Germany, 1997.
52. Sheldrick, G.M. Crystal structure refinement with SHELXL. *Acta Cryst. Sect. C Struct. Chem.* **2015**, *C71*, 3.